In Situ X-Ray Absorption Spectroscopy Studies of Functional Nanomaterials

5

Soma Chattopadhyay, Soon Gu Kwon, Elena V. Shevchenko, Jeffrey T. Miller, and Steve M. Heald

Contents

S. Chattopadhyay (✉)
Elgin Community College, Elgin, IL, USA
e-mail: soma.tifr@gmail.com

S. G. Kwon
Center for Nanoparticle Research, Institute for Basic Science and Seoul National University, Seoul, Republic of Korea

E. V. Shevchenko
Nanoscience and Technology division, Argonne National Laboratory, Argonne, IL, USA

J. T. Miller
School of Chemical Engineering, Purdue University, West Lafayette, IN, USA

S. M. Heald
Advanced Photon Source, Argonne National Laboratory, Argonne, IL, USA

C. S. S. R. Kumar (ed.), *In-situ Characterization Techniques for Nanomaterials*,
https://doi.org/10.1007/978-3-662-56322-9_5

1 Definition of the Topic

X-ray absorption spectroscopy (XAS) is a powerful technique to study the unoccupied states and the local structure around an excited species of atoms from an element present in a material. Recently, in situ XAS is being used to study catalytic transformations, synthesis of nanoparticles and thin films, kinetics of potential battery materials, etc. Such studies can explain the mechanisms associated with the formation of chemical species during various types of reactions. In this chapter, we shall describe how XAS has proved to be a powerful characterization tool for nanomaterials with potential applications by determining the variation in interatomic distances, coordination numbers, and the type of neighboring atoms within the first few coordination shells of the atom of interest in nanoparticles.

2 Overview

Nanomaterials defined as materials with at least one dimension in the nanometer ($1\ \text{nm} = 10^{-9}\ \text{m}$) range have been found to possess structure and properties that are significantly different from those of the corresponding bulk material. The large surface-to-volume ratio of nanoparticles (NP) makes their surface play a key role in tailoring their physical and chemical properties. Hence, they have been found to possess unique characteristics making them suitable for many novel applications related to energy storage, catalysis, electronic devices, drug delivery, etc. Studying such unique materials, so as to harness their properties for suitable applications, would need powerful characterization techniques.

Synchrotron-based X-ray absorption spectroscopy comprising of EXAFS (extended X-ray absorption fine structure) and XANES (X-ray absorption near edge structure) are exquisite characterization tools since they can study local structure around atoms in crystalline as well as amorphous and disordered materials and also in all states of matter. Hence, XAS is applicable and useful for nanomaterials related to condensed matter physics, engineering sciences, chemistry, biology, and environmental and geological sciences. Quick-XAS, i.e., Quick-EXAFS (QEXAFS) and Quick-XANES (QXANES) combined together, enables time-resolved spectroscopic studies down to millisecond regime and can provide information related to chemical changes and phase transitions taking place during the formation of NPs, cycling of batteries, catalytic reactions, physical transformations, and biological changes.

In this chapter, we shall describe how QEXAFS and QXANES have been successfully used to study mechanisms of chemical reactions and kinetics related to different types of NPs.

3 Introduction

The present century has seen a tremendous growth in the field of Nanotechnology. The ability to drastically change the physical and chemical properties of nanomaterials by changing their size and shape has increased their potential for many unique and useful applications relevant to modern times: high energy density batteries, catalysts for cars with high fuel efficiency, medical implants and drug delivery systems, computer chips related to miniaturization, materials for low-cost flat panel displays, elimination of environmental pollutants, etc. The growth of this emerging field has been possible due to novel synthesis routes that have been developed by scientists and engineers in the past decades. This coupled with the development of novel characterization tools and techniques that were initiated by the invention of the scanning tunneling microscope (STM) in the 1980s have further enriched the studies of nanomaterials of different types. Especially important for these nanomaterials have been the techniques based on synchrotron sources with a strong X-ray beam of high luminosity, which has made time-dependent studies possible in the fields of spectroscopy, scattering, diffraction, and imaging.

Standard X-ray absorption spectroscopy (XAS) scans at synchrotron sources were developed in the 1970s to study the detailed local structure around individual atoms from an element present in a compound [1]. These scans consist of step scans where the monochromator used to select the energy range is moved by a small amount in energy. Data are collected from the beginning to the end of the energy range till the entire spectrum for a particular element has been generated. Each of these scans generally takes 15–20 min. Quick-XAS measurements were developed in the mid-1990s at several synchrotron sources where data are collected on the fly, i.e., the monochromator motors are encoded and the crystals selecting the beam energy are moved with constant velocity from the beginning to the end of the energy range as the data are collected [2–7]. These scans have reduced the overhead time associated with moving the monochromator motor during step scans. Hence, a QEXAFS scan can be completed in 1–3 min and in some cases in several seconds. QXANES scans be collected in few seconds and sometimes in milli- and microseconds. Hence, time-resolved XAS studies have become possible and are becoming popular due to the unique combination of high penetration depth of hard X-ray beam and element sensitivity with time resolution. Apart from this, a new type of XAS called energy dispersive EXAFS (EDE) has been developed where a bent polychromator and a position-sensitive detector are used to collect data. The beam position is related to energy and the entire spectrum is collected in parallel. Here, the XAS spectrum can be collected in milliseconds, thereby making it extremely useful for studying catalytic reactions. Presently, research is being conducted to introduce ultrafast EXAFS and XANES also using pump probe methods [5].

Such developments related to QXAS have been extremely useful for in situ studies of various systems from different branches of science and engineering,

especially those related to the evolving field of nanotechnology. Nanomaterials have broad X-ray diffraction (XRD) peaks, and hence only limited structural information is available from XRD. In situ spectroscopy by itself as well as coupled with in situ scattering, imaging, and XRD can throw light on the pathways associated with synthesis of NPs and thereby help to produce tailor-made nano-systems in future for novel applications. In this chapter, we shall focus on how QXAS has already been used to study the local structural changes associated with (a) colloidal synthesis of NPs, (b) chemical reactions associated with homogeneous and heterogeneous catalysis, (c) synthesis of metallic NPs in nano-reactors, and (d) chemical changes occurring during cycling of battery materials.

4 EXAFS and XANES: Theory and Instrumentation

XAS is a powerful technique to study the local structure around an excited species of atoms. XAS in general consists of two regimes: (a) X-ray absorption near edge structure (XANES) and (b) extended X-ray absorption fine structure (EXAFS) [1, 8–12]. In general, EXAFS refers to the sinusoidal oscillations observed over a wide energy range extending to 1000 eV above the edge, while XANES refers to fine structure around an absorption edge extending typically 50 eV. XANES is strongly sensitive to the electronic levels around the Fermi level and hence provides information about the oxidation states and coordination geometries. EXAFS is used to determine the interatomic distances, variation in interatomic distances, coordination number, and the type of neighboring atoms within the first few coordination shells of the atom that is being studied by tuning the incident X-ray energy to the absorption edge of the atom.

A typical EXAFS spectrum is shown in Fig. 5.1a. X-ray photons of the specific energy chosen to interact with the atoms under study produce photoelectrons that are scattered by the neighboring atoms. The interference between the outgoing photoelectron wave and the scattered photoelectron wave at the probe atom causes oscillations in the absorption coefficient. EXAFS is defined as the normalized oscillatory part of the absorption coefficient above the absorption edge of the excited atoms in a material. Figure 5.1b shows the background subtracted data $\chi(k)$ in k-space. The Fourier transform of the normal oscillatory signal has peaks whose intensity depends on the type and number of atoms at a particular distance, and whose width depends on the structural disorder of the same atoms (Fig. 5.1c). The peak position represents the distance between the excited atom and the neighboring atom but occurs at slightly shorter distances than the corresponding theoretical bond length due to a phase shift, φ_j, between the incident and scattered waves. EXAFS spectra are modeled to obtain the average number, type, and distance of atoms around the probe atom, as well as mean square displacement of the average distance (σ^2). Figure 5.1d shows the pre-edge region of the EXAFS spectrum: the energy change is referred to as the edge jump. This region between −50 eV and +50 eV around the edge region is called XANES.

When the energy of incident X-rays photons (E) is scanned across the binding energy of a core shell electron, there is a sharp increase in the probability for X-ray to

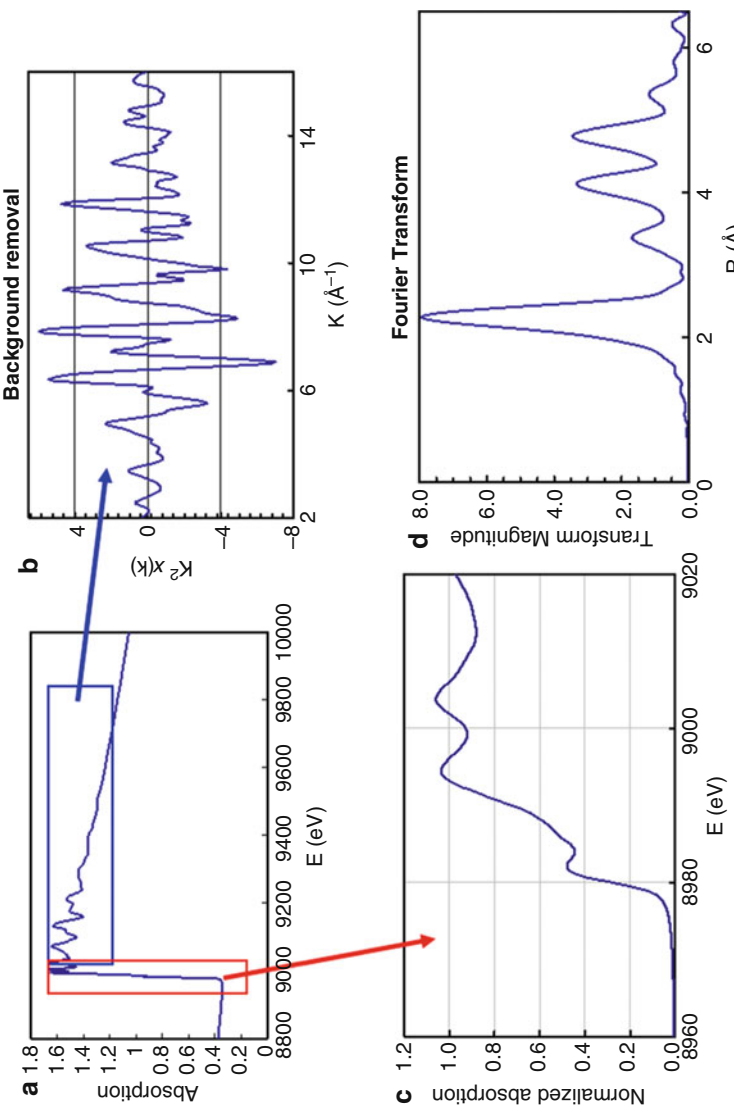

Fig. 5.1 (**a**) A typical EXAFS spectrum. (**b**) The background subtracted data in reciprocal space. (**c**) XANES region of the spectrum and (**d**) Fourier transformed EXAFS spectrum

be absorbed (μ), resulting in an absorption edge. The absorbed X-ray results in an excited atomic state consisting of a core hole and photoelectron. The photoelectron propagates as a wave with the wave number k,

$$k = \sqrt{2m(E - E_0)/\hbar^2} \tag{5.1}$$

where $\hbar = h/2\pi$ with h being the Planck constant, E_0 is at the absorption edge, and m is the electron mass. If the absorbing atoms are isolated (such as in an inert gas), μ has a relatively smooth atomic background (μ_0). On the other hand, if surrounding atoms exist as in solids, the photoelectron wave is scattered by them, and the outgoing and backscattered electron waves interfere, resulting a modulation of the absorption coefficient μ written as

$$\mu = \mu_0[1 + \chi(k)] \tag{5.2}$$

These modulations in $\chi(k)$ are called EXAFS and expressed as a sum of the sinusoidal functions from the scattering paths from all the neighboring atoms as

$$\chi(k) = \sum_{j=1} A_j(k) \sin\left(2kR_j + \varphi_j\right) \tag{5.3}$$

$$A_j(k) = \frac{N_j}{kR_j^2} S_0^2 F_j(k) e^{-2R_j/\lambda} e^{-2k^2\sigma_j^2} \tag{5.4}$$

and φ_j being the phase shift from the potentials of the absorber and backscattering atoms. These phase shifts are approximately linear and thus, the individual contributions maintain their sinusoidal character.

EXAFS analysis gives structural information around the absorbing atoms including number of neighbors (N_j), bond length (R_j), and the bond length distribution characterized by a Debye-Waller factor (σ_j^2). Since the mean free paths (λ) of the electrons are usually short, information is limited to a few Å around absorbing atoms; therefore, EXAFS is a local structural probe. Particularly important are the backscattering functions $F_j(k)$ and phase shift φ_j, which are characteristic of the atomic species of the scattering atoms; thus, EXAFS analysis can distinguish between several types of atoms which may be present in a compound. The Fourier transform of k-weighted $\chi(k)$ separates the signal in terms of the radial distances (R_j) between the absorbing atom and its neighbors. The peak height depends on the type and number of atoms at a particular distance and the peak width depends on the structural disorder (σ_j^2) of the atoms at that distance. EXAFS data can be modeled to obtain N_j, R_j, and σ_j^2 for the first few coordination shells.

A typical setup for performing QXAS measurements is shown in Fig. 5.2. The X-ray beam from the synchrotron source goes through a double a crystal monochromator which selects the energy range needed for the element of interest. The beam then passes through filters and a harmonic rejection (HR) mirror. The latter is used to eliminate higher energy X-rays. Most HR mirrors consist of Rhodium, Platinum, and

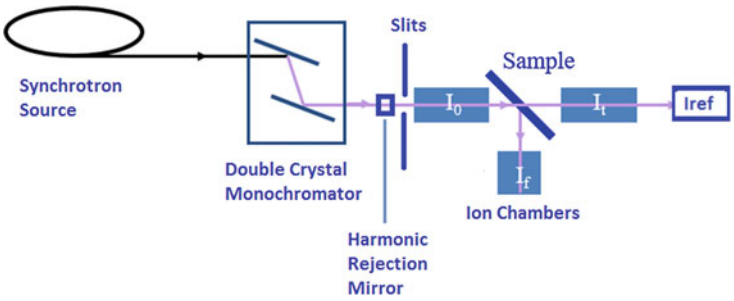

Fig. 5.2 A typical XAS setup in a beamline

glass stripes for use in different energy ranges. The beam is then defined with the help of mechanical slits and passes through the incident ion chamber (I_0) that counts the number of photons falling on the sample. Size of incident beam is always kept smaller than the size of the sample. Concentrated samples are placed perpendicular to the beam, whereas dilute samples are placed at 45° to the path of the beam to allow for fluorescence detection. For homogenous, highly concentrated samples, μ is measured with transmission geometry and obtained from Beer's law as

$$\mu x = \ln(I_0/I_t) \tag{5.5}$$

where x is thickness of the sample, and I_0 and I_t are incident and transmitted X-ray intensity, respectively. For diluted samples, the fluorescence signal is used to obtain μ since the fluorescence intensity is proportional to the number of core-holes created by X-ray absorption and thus proportional to the absorption coefficient. It is more sensitive than transmission mode because fluorescence comes only from the element of interest. The transmission ion chamber (I_t) counts the number of photons in the beam after passing through the sample. Fluorescence X-ray from dilute samples is detected with an ion chamber (I_f) placed at 90° to the incident beam. These ion chambers are equipped with filters and Soller slits to minimize the background. I_{ref} is the reference ion chamber placed after the transmission ion chamber.

A metal foil of the element which is being probed is placed on this ion chamber so as to verify the calibration of the edge energies before merging the scans. The foil scans are important since the amplitude $\left(S_0^2\right)$ needed to fit the data for a particular element is obtained by fitting the EXAFS data from the respective foil. $\left(S_0^2\right)$ can depend on chemical environment and is energy dependent. However, it mainly comes from the atomic nature of the central atom, and these dependencies are small. The gases in the ionization chamber were optimized on the basis of the X-ray energy so that 1–5% of the X-ray gets absorbed in I_0, 70% in I_t, and the rest in I_{ref}. Energy calibration is done before data are taken at each edge energy. Solid samples are ground to fine powder with the particle size much less than one absorption length ($1/\mu \sim 40$ μm) to avoid the pinhole effect. The powder can be

rubbed on Kapton® tapes and stacked with the number of layers optimized so that the edge step ($\Delta\mu x$) at a particular edge energy becomes 0.5 ~ 1, the total absorption by the entire sample ($\mu_{total}x$) is less than 2.5, and absorption by the respective atom ($\mu_{element}x$) is about unity. Powder can also be mixed with the correct amount of fine powder of boron nitride and pressed into pellets so as to have the right edge step and absorption. Over 10 scans are recorded for each edge energy measured for a sample to ensure repeatability and averaged to improve statistics.

The data are processed using Athena [13]. Conventional EXAFS analysis consists of extracting the oscillations, $\chi(k)$, as a function of the photoelectron wave number (k) from the background-subtracted absorption spectrum, $\mu(E)$, and Fourier-transforming $\chi(k)$ into real space, $\chi(R)$. The measured absorption spectrum below the pre-edge region is fitted to a straight line. The background contribution above the postedge region is fitted to a cubic spline (a segmented third order polynomial). The fitted polynomials are extrapolated through the total energy region and subtracted from the total absorption spectra. The theoretical paths are generated using FEFF6 [14], and the models are constructed in the conventional way using the fitting program Artemis [13] to refine the fitting parameters. The background subtracted $\chi(R)$ data are fitted to models based on the FEFF-based calculations of the scattering paths using the relevant coordination numbers, Debye-Waller factor (σ^2), and bond lengths as parameters. Various scattering models and different fit ranges are tried using the Artemis fitting program, before arriving at the best fit.

5 Key Research Findings

Nanometer-sized particles in the form of loose aggregates, wires, spheres, and various other shapes and sizes have been found to possess superior structural, optical, electronic, and magnetic properties in many cases making them suitable candidates for versatile applications in new technological devices. Progress in instrumentation and detectors at the synchrotron sources in the last two decades has led to new and powerful characterization tools to probe the structure of materials. Especially novel and useful has been the invention of the time-resolved techniques in the field of high-resolution X-ray diffraction (HRXRD), small-angle X-ray scattering (SAXS), pair distribution function (PDF), imaging, and quick X-ray absorption spectroscopy (QXAS). These techniques have become critical to the research efforts in the field of nanomaterials. They have the ability to generate real-time structural data and can help to identify how structure influences the functional properties and performance of devices made from these nanomaterials. Hence, these advanced characterization methods have led to the development of new synthesis techniques for NPs and thin films. They have also helped in studying chemical and physical processes occurring in catalysis, energy storage in batteries, protein formations, mechanically stressed nano-alloys, etc. We shall describe how QXAS, either alone or in combination with HRXRD, SAXS, PDF, and other techniques, can help to enhance the study of advanced materials in various fields and their performance.

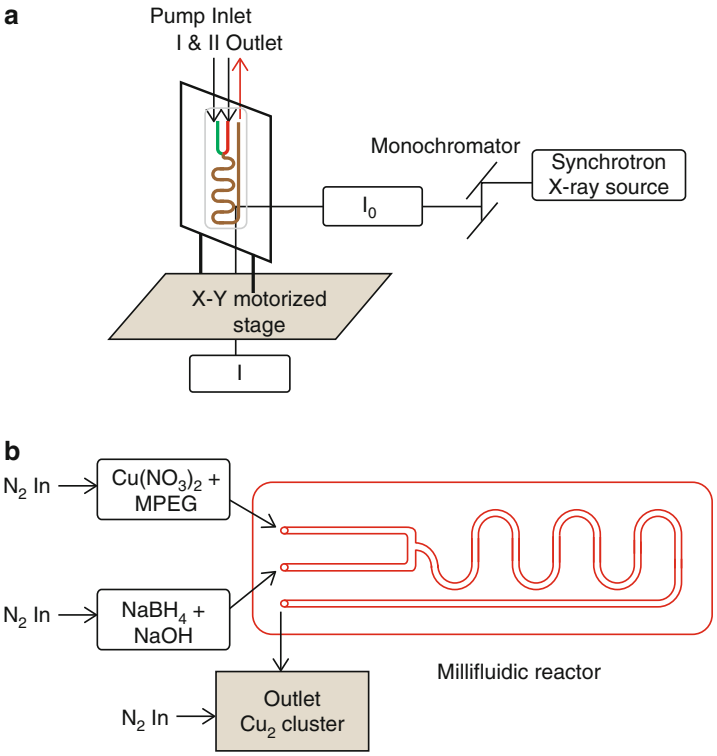

Fig. 5.3 (**a**) QXAS setup for microfluidic chip reactor in the beam with the beam coming from the right and the Stern-Heald detector placed at 90° to the beam. (**b**) The microfluidic chip reactor with the inlet tubes to introduce the precursors and the outlet tube for the clusters to come out and get collected for further characterization

5.1 Using In Situ XAS to Study Synthesis of Nanoclusters and Nanoparticles in the Beam

5.1.1 Metal Nanoclusters Using Milli−/Micro-Fluidic Chip Reactors

Recently, millifluid and microfluid reactors are being used for the preparation of NPs [15–21]. These lab-on-a-chip reactors consisting of small channels with micrometer diameter have liquid precursors flowing through them. They are allowed to react and produce NPs or nanoclusters. The use of time-resolved QXAS in conjunction with microfluidic lab-on-a-chip reactor has helped in studying the reaction dynamics of a chemical reaction at every stage during the formation of NPs.

A typical QXAS setup for chip-based microfluidic experiment on the beamline to produce copper nanoclusters [18] is shown in Fig. 5.3a, where the beam is scanned in a raster fashion over the microfluidic reactor while data are being collected at different points of the reactor with serpentine channels shown in Fig. 5.3b from the time of introducing the precursors to the end of the reaction where Cu nanoclusters come out

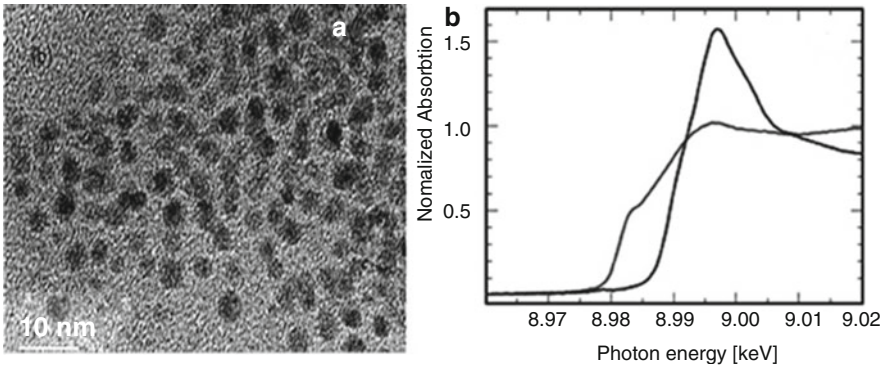

Fig. 5.4 (**a**) TEM image of ultra-small copper nanometer-sized clusters collected at the outlet of a millifluidic reactor. (**b**) QXANES spectra of Cu precursor (peak with higher absorption) versus Cu nanoclusters (peak with lower absorption) [18]

of the reactor. The nanoclusters are further characterized by transmission electron microscopy (TEM) and UV-vis absorption spectroscopy.

Figure 5.4a shows a TEM image of ultra-small Cu nanoclusters (UCNCs). Figure 5.4b compares the QXANES spectrum taken for $Cu(NO_3)_2.xH_2O$ precursor at the inlet to the spectrum for UCNCs at the outlet. EXAFS spectrum was taken every 30 s and at several positions along the path of the chip reactor to track the nanocluster formation process. Analysis of QXAS data helped in the determination of size, oxidation state, coordination number, and bond length of the UCNCs at various stages of their formation in the reactor and confirmed that oxidative impurities were not present in the sample collected from the outlet. These clusters, smallest ever produced using a lab-on-a-chip reactor, have been found to efficiently catalyze C-H oxidation reactions when supported on silica. In situ QXAS, proved to be an useful tool to study the controlled synthesis of Cu nanoclusters that were found to catalyze C-H oxidation for the first time, later was used successfully to study the formation of Au and Pt nanocluster also [19, 21]. Such studies will provide fundamental insights into formation of novel nanoclusters and NPs which will help to develop the next generation of high-performance advanced materials.

5.1.2 Synthesis of Colloidal Metal, Metal-Oxide, and Doped Metal-Oxide Nanoparticles

The exponential growth in the field of nanotechnology in the past two decades has led to the development of novel synthesis techniques in this field. One of them is the colloidal route which has helped to produce stable nanocrystals of metals, semiconductors, and insulators with uniform size distribution and of different shapes and sizes for a variety of applications [22–26]. Colloidal NPs generally possess an inorganic core surrounded by surfactants or ligands which are used in stabilizing them. Each individual colloidal nanocrystal is a freestanding nanoparticle in solution. Though the process of doping has been known for a long time, doping the

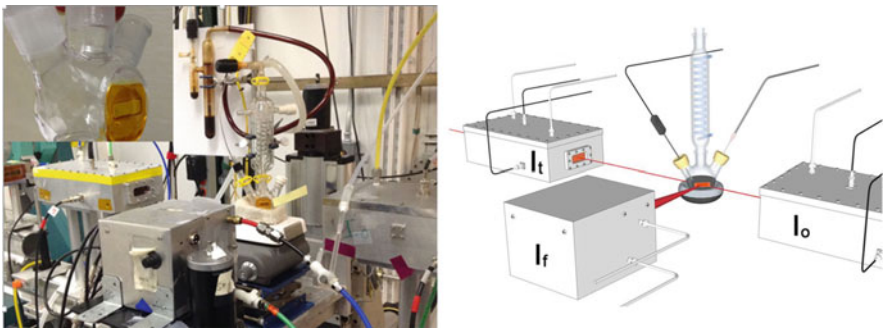

Fig. 5.5 QXAS setup for in situ X-ray absorption spectroscopy measurement of the synthesis of pure and Mo-doped hollow iron oxide NPs. The picture on the left shows the actual Schlenk-line setup installed at the beamline located at Advanced Photon Source, USA. The schematic diagram on the right shows the path of the X-ray beam and the arrangement of the detectors: I_o, I_t, and I_f for measuring intensities of incident, transmitted, and fluorescent X-rays, respectively [27]

colloidal nanocrystals has been challenging. The synthesis process of pure and doped nanocrystals involves several steps [24] and heating the solution to higher temperatures. Controlling each of these steps is crucial for obtaining the right size and shape for the desired NPs. Though there has been substantial progress in the synthesis of doped NPs, the doping mechanisms have been mainly studied by ex situ techniques, including TEM, Fourier transform infrared spectroscopy (FTIR), UV-vis absorption spectroscopy, Raman, etc., that do not provide detailed information on the kinetics of the doping mechanism. Successful synthesis of doped NPs requires studying the correlation of various kinetic parameters. Therefore, time-resolved studies of the doping processes are critical to resolve the doping mechanism in colloidal NPs.

Recently, the entire process of Mo-doped and un-doped iron oxide NPs synthesis was studied in real time by synchrotron in situ X-ray absorption spectroscopy done in QXAS mode [27]. The actual and schematic setup for this experiment is shown in Fig. 5.5. Mo-doped iron oxide NPs have been chosen since it is a promising electrode material to improve Li^+ ion capacity of rechargeable battery. XAS being a unique characterization technique, the QXAS measurements done at Fe edge as well as at Mo edge during the synthesis allowed simultaneous monitoring of reaction kinetics of the precursors, compositional changes of the NPs during the synthesis, the chemical state (valency and coordination geometry) and position (whether it is in the solution or in the host lattice) of the dopant. TEM images of the colloidal metallic iron NPs before oxidation to hollow iron oxide NPs and the Mo-doped iron oxide NPs produced in the beamline at the end of the synthesis are shown in Fig. 5.6.

The QXANES data along with the linear combination fit results are shown in Fig. 5.7. The analysis of the time-resolved XAS studies coupled with TEM measurements revealed for the first time an *oxidation induced doping mechanism* which is illustrated in Fig. 5.8b corresponding to the chemical reaction shown in Fig. 5.8a. The reaction mechanism from QXAS results predicts that the mass transport of the

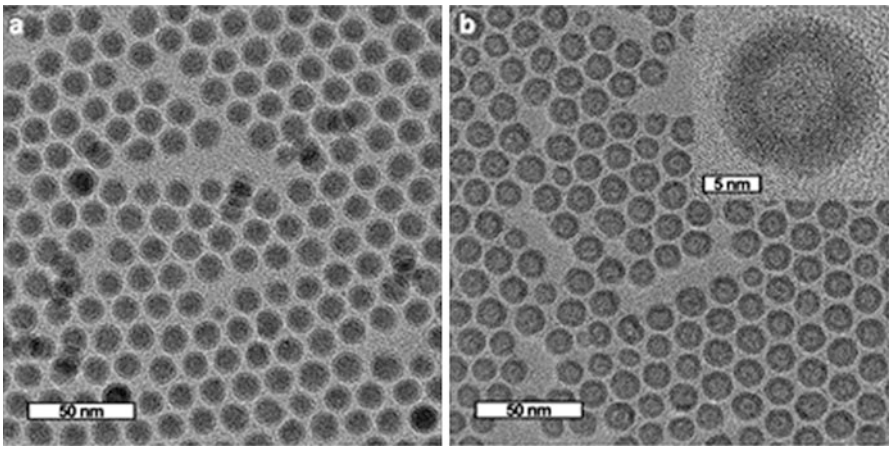

Fig. 5.6 (**a**) TEM image of the iron NPs before oxidation, (**b**) TEM image of Mo-doped iron oxide NPs after oxidation [27]

host (iron and oxygen) atoms induces the incorporation and internalization of the dopant atoms (molybdenum) into the lattice of oxidized hollow NPs of γ-Fe_2O_3. Time-resolved QXANES/QEXAFS study revealed that the reaction kinetics of the nucleation, growth, and oxidation of the host NPs are significantly affected by the dopant precursor, and the latter can substantially change the reaction kinetics of formation of iron and iron oxide NPs. Thus, in the presence of dopant precursor, we observed significantly faster decomposition rate of iron precursors and substantial resistance and higher stability of iron NPs against oxidation. The same doping mechanism and higher stability of host metal NPs against oxidation was observed for cobalt-based systems also. Since the internalization of the adsorbed dopant at the surface of the host NPs is driven by the mass transport of the host, this mechanism can be potentially applied to introduce dopants into different oxidized forms of metal and metal alloy NPs providing the extra degree of compositional control in material design. This is the first time that an entire synthetic colloidal chemistry was done successfully at a beamline demonstrating and proving that NPs can be synthesized in organic solutions with only inorganic capping ligands. We believe that oxidation-induced doping mechanism can be applied to a number of other NP systems where the mass transport can be induced chemically (e.g., oxidation) or electrochemically. This in situ measurement technique is generally applicable for time-resolved mechanism study of various doped NPs synthesis using the conventional reaction setups that are generally used in the laboratory, and it proves the strength of QXAS in being able to provide insight into chemical reactions. It should be possible to use QXAS to monitor synthesis of NPs by sol-gel, microemulsion, and other wet chemical techniques also.

Apart from these, there have been reports of QXANES being used successfully to study the in situ growth of ZnO nanowires from zinc nitrate and HMTA (hexamethylenetetramine) precursors during chemical bath deposition (CBD) for a fundamental

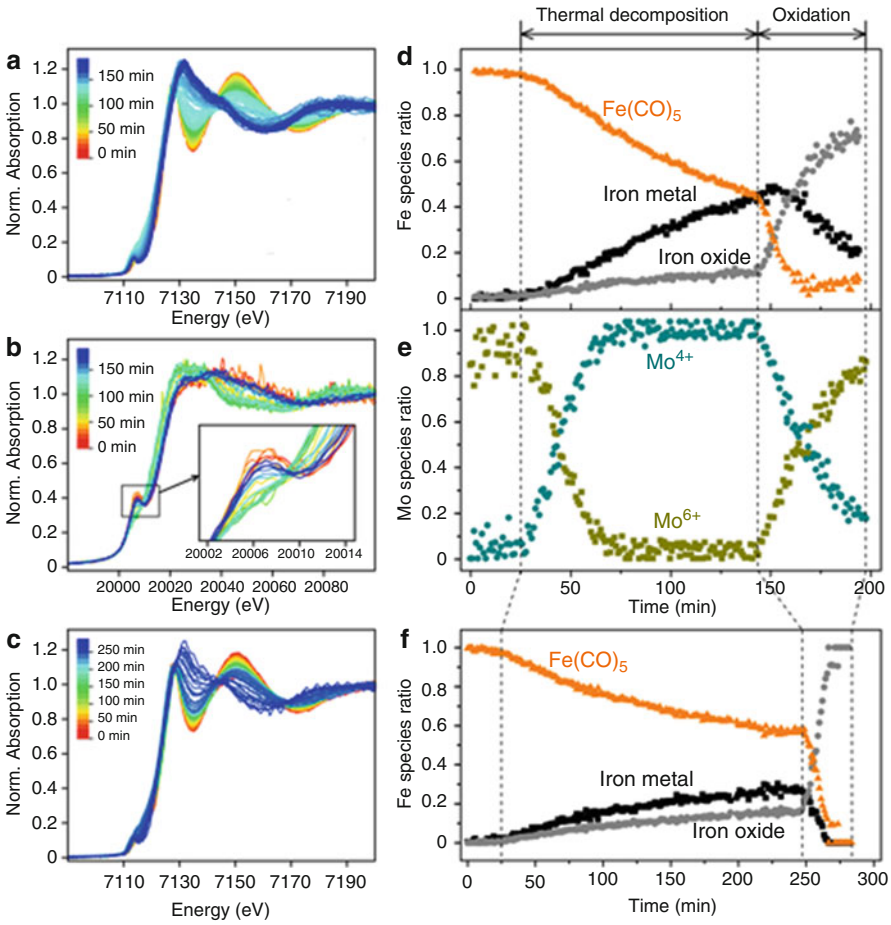

Fig. 5.7 Time-dependent changes of Fe and Mo XANES spectra and the ratio of iron and molybdenum species during the synthesis of Mo-doped and un-doped hollow iron oxide NPs. (**a**, **b**): Fe-QXANES and Mo-QXANES spectra, respectively, taken during the synthesis of Mo-doped hollow iron oxide NPs. The inset in panel b shows the magnified pre-edge peak range. (**c**) Fe *K*-edge QXANES spectra acquired during the synthesis of un-doped hollow iron oxide NPs. (**d**, **e**) Linear combination fit results obtained from the time-dependent XANES spectra (**a**) and (**b**), respectively, showing the changes in the ratio of iron and molybdenum species, in the reaction mixture as a function of time during the synthesis of Mo-doped hollow iron oxide NPs. The reaction temperature reached 180 °C at 37 min. (**f**) Time-dependent change of iron species obtained from linear combination fits of QXANES spectra taken during the synthesis of un-doped hollow iron oxide NPs. The reaction temperature reached 180 °C at 32 min (More details of the experiments and analysis can be found in Ref. 27)

understanding of the reaction mechanisms and kinetics associated with the underlying chemical processes [28]. In situ QXAS has been used to study the 2-stage growth mechanism associated with the aqueous synthesis of glutathione (GSH) capped ZnSe quantum dots [29]. It has also been used to monitor the adsorption of Co^{2+} on the

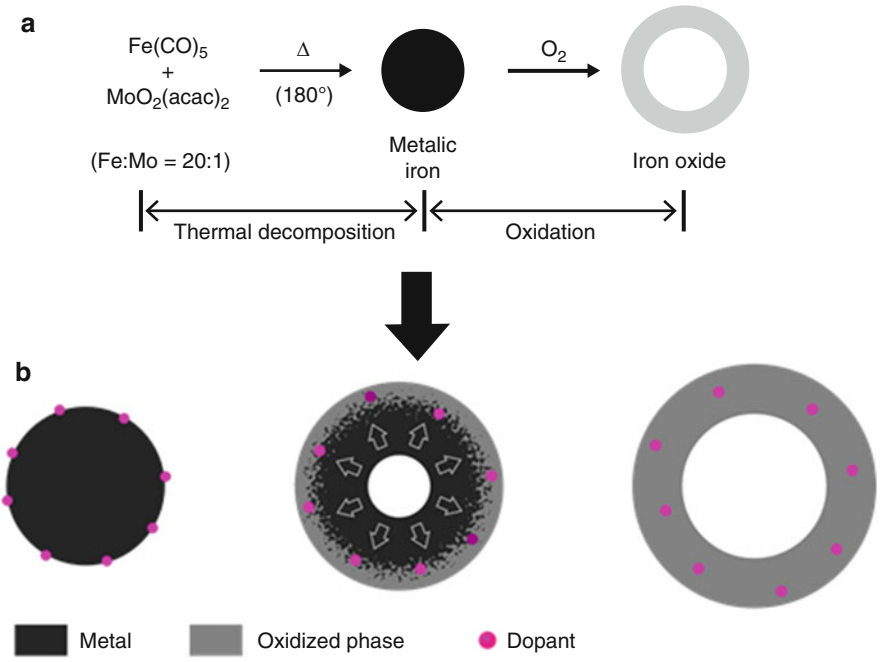

Fig. 5.8 (**a**) Synthesis of Mo-doped iron oxide hollow shell NPs. (**b**) Modeling of the chemistry associated with oxidation-induced doping mechanism as predicted from QXAS results. A metallic iron NP with dopant ions adsorbed on the surface (left); early stage of the oxidation of metallic Fe NP and capturing of Mo-dopant ions inside of the oxidized layer (middle); doped hollow shell NP after full oxidation (right)

surface of Fe_3O_4 NPs in high temperature aqueous fluids [30]. The results have indicated that QXAS with its capability to determine the coordination environment around individual atoms, will enable discovery of novel synthesis routes for new materials in future.

5.2 In Situ QXAS Studies of Nanomaterials for Battery Applications

The enormous energy need of our civilization is the driving force behind the intensive research of materials related to energy-storage. There has been huge progress in the field of battery materials in the last two decades due to the growing demand of modern technology. Since their discovery in the early1990s, Lithium ion batteries have become popular since they possess the highest energy density of all rechargeable batteries available in the market and hence have become standard power source for many electronic devices like cell phones, laptops, etc. Further research to improve the properties of these batteries has been ongoing since they may be the source of power for a future generation electric vehicles and large-scale

electrical grid storage also. XAS especially QEXAFS and QXANES have proved to be powerful and ideal tools to study batteries. Together, they have the capability to correlate the changes in the electronic state of an atom to the structural changes occurring in the neighborhood of an atom during electrochemical changes, i.e., charging and discharging of batteries. QXAS can provide valuable insight about the mechanisms in electrochemical reactions when one of the transition metal constituents is removed or changed in the electrode materials, which is needed to achieve high specific capacity and long-term stability in Li-ion batteries. Hence, they have been used for past 20 years to probe the structure and composition of various types of electrode materials used in batteries [31–50]. These studies have thrown light on the charge compensation process during cycling of batteries and the response of cathodes to Li ion insertion and extraction. It has been observed that for transition metal doped $LiCoO_2$ (a) capacity fading is closely related to the J-T distortion of the NiO6 octahedron when Ni is doped at Co sites in $LiCoO_2$ and (b) during electrochemical delithiation process, all the charge compensation occurs at the Ni site which changes oxidation state from 3+ to 4+ during charging, thereby causing reduction of J-T effects. Co atoms oxidize towards the end of charging process [37–40]. Studies of $LiMn_2O_4$ layered compounds have shown that Li de-intercalation leads to oxidation of Mn^{3+} to Mn^{4+} to MnO_2, and there are local structural changes around Mn atoms which can cause cyclic instability of the battery material [32, 34, 36]. The active role of oxygen atoms during cycling of batteries is confirmed. This research has proved that with proper design of electrodes and choice of active materials, lithium-ion batteries can function at high rates and with higher utilization of the active material. These studies have opened the path for development of lithium-iron phosphate [46] and other high capacity cathode materials [47, 48] and also intermetallic-phase-based anode materials with the zinc blende structure [35].

Significant improvement is still needed in this field to produce electrode materials which are cheap, safe-to-use, and possess higher capacity and higher rate performance. Use of nanomaterials as electrodes for batteries is being probed since NPs have more surface area which will give them higher charge and discharge rates, short path length for electron and Li ion transport, and higher strain accommodation capacity. In situ XAS on nanometer-sized materials were reported as early as 2010 when the Cu *K*-edge of 20 nm sized 85 wt% CuF_2–15 wt% MoO_3 nanocomposite was investigated [51] to study the electrochemical conversion reaction in metal fluorides which have demonstrated high energy density. The nanocomposite, prepared by high energy milling, resulted in the formation of highly dispersed metallic Cu NPs with size 2–3 nm as a result of the lithiation reaction, i.e., conversion of CuF_2 into Cu and LiF during discharge of the battery. In situ XAS studies of batteries with NPs of metallic Sn, SnO_2, and hybrid $Sn_3O_2(OH)_2$/graphite as anode material show segregation of tin and formation of SnLi and Li_2O phases within the electrodes. Though SnO_2 has been found to be a more promising candidate than metallic tin, QXAS studies of the tin atoms during the battery cycling process helped to explain the poor electrochemical performance and rapid capacity decline of the batteries using both Sn and SnO_2 [52, 53]. In situ QXAS measurements to track structural changes during Li intercalation/de-intercalation of nanometer-sized

$LiCoO_2$ demonstrated enhanced capacity fading and irreversible losses due to high surface area of the NPs [54]. In situ XANES studies of Ni edge and Mo edge of MoO_2 NPs doped with 2 atomic percent of Ni showed the nucleation of the ternary Ni:MoO_2 compound formed by substitution of Mo atoms by divalent Ni atoms. Doubling of the initial discharge capacity has been observed in these Ni-doped nanometer-sized MoO_2 due to relaxation of local structure. An increase of capacity for both pure and Ni doped MoO_2 anodes also occurred upon cycling with increasing cycling rate [47]. Nanocomposites of LiF/V_2O_5 (0–20 wt% of V_2O_5) prepared by high energy ball-milling showed stable capacity over a period of 20 cycles for the sample with 15 wt% of V_2O_5. In situ Fe and V edge XAS data helped to diagnose the oxidation states of V and Fe atoms and identify the new phases and the mechanism of their formation during the battery cycling [48]. In situ XAS demonstrated that Cu^{2+} copper ions in 2D–layered copper birnessite NP electrodes get reduced to amorphous nanosized copper metal which can get oxidized to Cu^{2+} ions during lithium insertion and de-insertion cycle leading to enhanced discharge capacity of these layered Mn oxide compounds when compared with the compounds without copper [55].

Research using in situ XAS has been extended to hollow iron-oxide NPs whose electrochemical properties have been investigated to probe their usefulness as an anode and a cathode material in Li ion batteries [56, 57]. The aim was to study if changing the morphology of NPs to something other than solid NPs can lead to enhanced properties of the batteries constructed from them. Better performance was observed for the smaller sized hollow iron oxide NPs compared to the bigger sized NPs with the same high stability when cycled in high voltage ranges [56]. Cation vacancies in octahedral sites of hollow γ-Fe_2O_3 NPs can serve as hosts for Li ions at high voltage range and possess high capacity, excellent Coulombic efficiency, good capacity retention, and superior rate performance demonstrating that this material can be successfully used as a cathode material for Li ion batteries. The studies of Koo et al. showed that hollow core-shell NPs can be used efficiently for reversible Li ion intercalation without causing structural changes in the material and provided a clear understanding of the lithium intercalation processes during electrochemical cycling. Cation vacancies in hollow γ-Fe_2O_3 NPs can be utilized for fast transport of sodium ions also and produce low-cost rechargeable cathodes with excellent charge transport properties [58]. Figure 5.9a shows a TEM image of hollow γ-Fe_2O_3 NPs after annealing of Fe/Fe_3O_4 core-shell NPs for 12 h at 200 °C. Figure 5.9b depicts the fabrication of light-weight, binder-free, flexible, and stable electrodes with carbon nanotubes (CNTs). Figure 5.10 shows the in situ QEXAFS measurements done at Fe k-edge during charging and discharging of the battery several times and over a period of few hours in the beam. Figure 5.10a shows the voltage profile of the first electrode discharge versus metallic sodium counter electrode. The points marked in Fig. 5.10a correspond to the in situ QXANES data collected at Fe edge during charging and discharging of the battery. Figure 5.10c shows the Fourier transformed QEXAFS data and depicts the changes in Fe-O and Fe-Fe bond distances during intercalation of Na ions into the hollow iron oxide NPs. Linear combination of the QXANES data was used to generate the plot of Fig. 5.10d showing the Fe-oxidation state during the cycling of the battery. This study proved

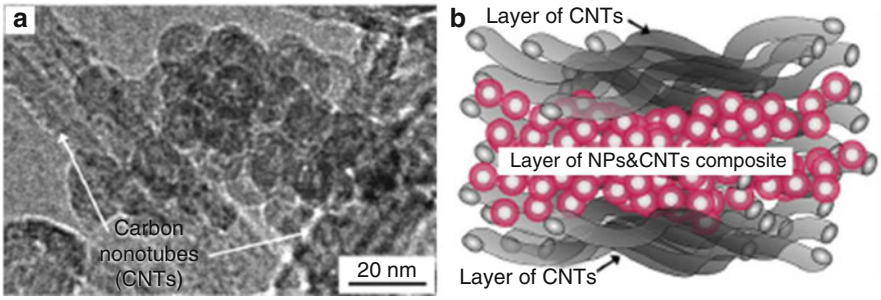

Fig. 5.9 (**a**) TEM image of showing formation of hollow γ-Fe_2O_3 NPs, (**b**) fabrication of low- cost, stable electrodes with NPs and CNTs [58]

that CNTs are successful as a conductive matrix for NPs, which can be used as high performance cathodes with Na + ions. Thus, we see that QXAS with its unique ability to probe local structure around individual atoms and the oxidation state of the element has proved to be extremely useful in understanding structure-property correlations in energy related materials. It has helped to discover new materials with enhanced electrical properties, thereby expanding the ongoing research of NPs as potential materials for next generation batteries.

5.3 In Situ QXAS Studies of Reactions in Catalytic Nanomaterials

Catalysts are compounds that affect the pathway and mechanism of a chemical reaction but do not enter the overall stoichiometry of the reaction. From the time of its discovery by Berzelius in 1835, catalysis has been known to play an important role in chemistry as many chemical processes involve catalysts at some step. The exponential growth in the field of nanotechnology has led to the discovery of novel synthesis techniques in the last two decades. This has not only initiated the research for advanced characterization techniques but has also revolutionized the field of catalysis since catalytic properties depend strongly on the number of surface atoms, which are enhanced in nanometer-sized particles. Nanocatalysts in the form of metals, metal oxides, metal complexes, biocatalysts, as well as other types of compounds have played a major role in water gas shift reactions, CO oxidation, hydrogenation, etc., as well as in fuel cells, energy conversion, and storage technologies. The catalytic properties of materials are determined not only by their size and shape but also by their composition and structure, the type of organic capping agent, the properties of inorganic support, etc. When a catalyst is active, there are changes in its physical and electronic properties. In order to be able to control the functions of engineered NP catalysts, detailed understanding of the relationships between the physical and electronic structure and the catalytic activity is essential. XAS has proved to be an ideal tool for catalysts since the powerful X-ray beam can penetrate matter in all three states as well as both amorphous and crystalline materials. It can

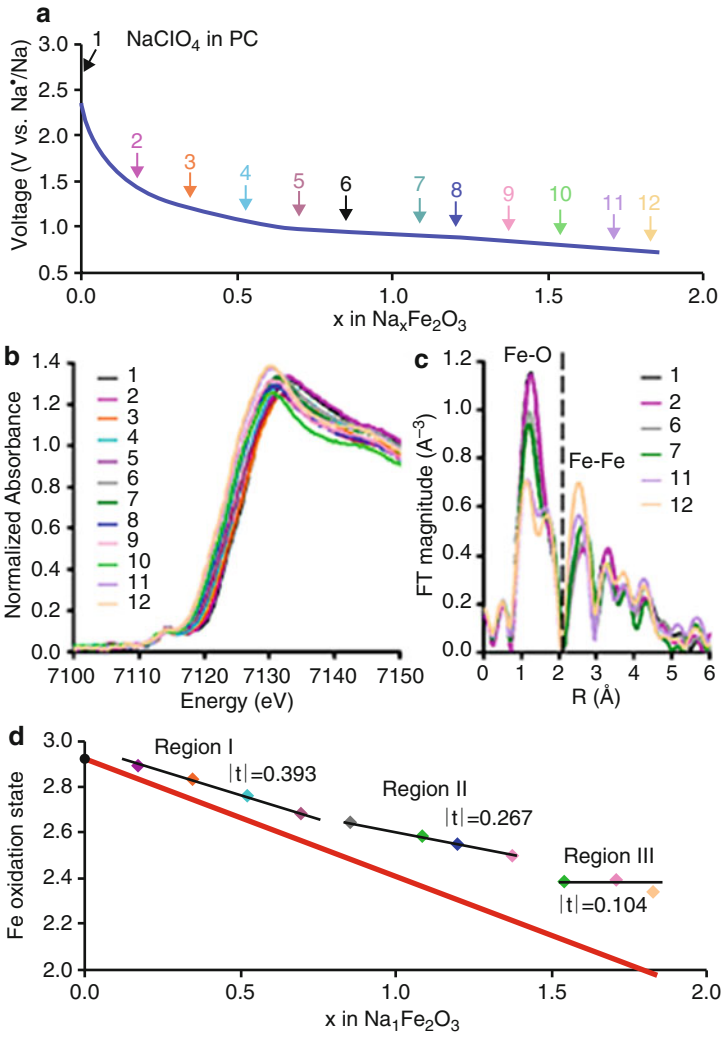

Fig. 5.10 (**a**) Voltage profile of first electrode discharge versus metallic sodium counter electrode; (**b**) QXANES data corresponding to the points shown in (**a**); (**c**) Fourier transformed QEXAFS data and (**d**) oxidation state of Fe obtained from the QXANES plots in (**b**) [58]

provide information about physical and electronic property changes occurring during reactions under changing conditions of pressure, temperature, and the flow of a multitude of gases needed for catalytic reactions. With fluorescence measurements, it can also detect species present at very low concentrations. Hereby, we shall present how results generated from in situ XAS research has helped to study homogeneous and heterogeneous catalysts of nanometer-sized metals, metal-oxides, etc., and paved the road for designing nanocatalysts with novel properties.

Though XAS has been used since the 1980s for studying catalysts [59], in operando studies were started during the late 1990s. Mukerjee et al. reported one of the earliest in operando XAS studies done on Pt and Sn edges to study the effects of Sn substitution during voltage cycling of carbon-supported Pt electro-catalysts [60]. Since then, there have been several review articles [61–82] on in situ XAS experiments that were conducted successfully at different synchrotron sources to study electro-catalysts, homogeneous, and heterogeneous catalysts that include metallic, bi–metallic NPs and nanoclusters, zeolites, oxides, and supported catalysts. These experiments have helped in identifying reaction intermediates and catalysis active sites. In situ XAS studies have worked successfully for fuel cells, water-gas experiments, and in operando cells. Researchers have developed theories (DFT) to explain the behavior of the catalysts and have designed catalysis setups [67, 68, 83–88] for re-enacting conditions that exist in industries. In order to do in situ measurements of catalysts similar to industrial atmosphere, Bare et al. [84] developed and implemented a four-channel ionization chamber with two different in situ cells. This setup shown in Fig. 5.11 helps in collecting QXAS data from 4 samples simultaneously in transmission geometry, thereby eliminating scan-to-scan uncertainties. In addition to increased productivity and time-saving, this setup has enabled in situ XAS data collection axially at four different positions in a catalyst bed and decipher small differences in the behavior of similarly prepared catalysts. Apart from that, catalysts can be subjected to same conditions of temperature and gas pressure and reference spectra can be collected in four channels simultaneously. This setup is easy-to-use and can be used in bending magnet and wiggler beamlines with a horizontal fan of radiation.

Rochet et al. have developed a cell to conduct in situ and operando experiments to improve cycle length, catalytic activity, and selectivity towards heavy paraffin of Fischer-Tropsch supported cobalt nanometer-sized catalysts [86]. They have been successful in doing QXAS under realistic working conditions at high pressure (18 bar of syngas) and reaction temperature (250 °C) under pure hydrogen at 400 °C, thereby proving that it is possible to mimic harsh conditions in a real catalytic fixed bed reactor. An operando QXAS cell has been developed by O'Neill et al. to measure simultaneous changes in catalyst structure and catalytic activity during liquid phase hydrogenation of furfural over supported copper catalysts [87]. This setup allowed continuous monitoring of the size of the copper NPs whose sintering has been proved to be predominant mode of catalyst deactivation for a $Cu/\gamma\text{-}Al_2O_3$ catalyst. Detailed description of several catalysis cells has been given by Bare and Ressler in their chapter on catalysis [67]. The developments in instrumentation related to in situ QAS at various beamlines all over the world have immensely helped the catalysis community. Kumar et al. have studied multicomponent NiFeCu catalyst using in situ XAS coupled with scanning electron microscopy (SEM), FTIR, and X-ray photoelectron spectroscopy (XPS) [89]. The results demonstrate that though the NiFeCu catalyst appears homogeneous at the mesoscale, it is highly heterogeneous at the nanoscale. There are changes in the oxidation states of Ni, Fe, and Cu during reaction. Cu was fully reduced before reaction and later became partly oxidized upon exposure to ethanol and oxygen. Ni is mostly (75%) reduced and does

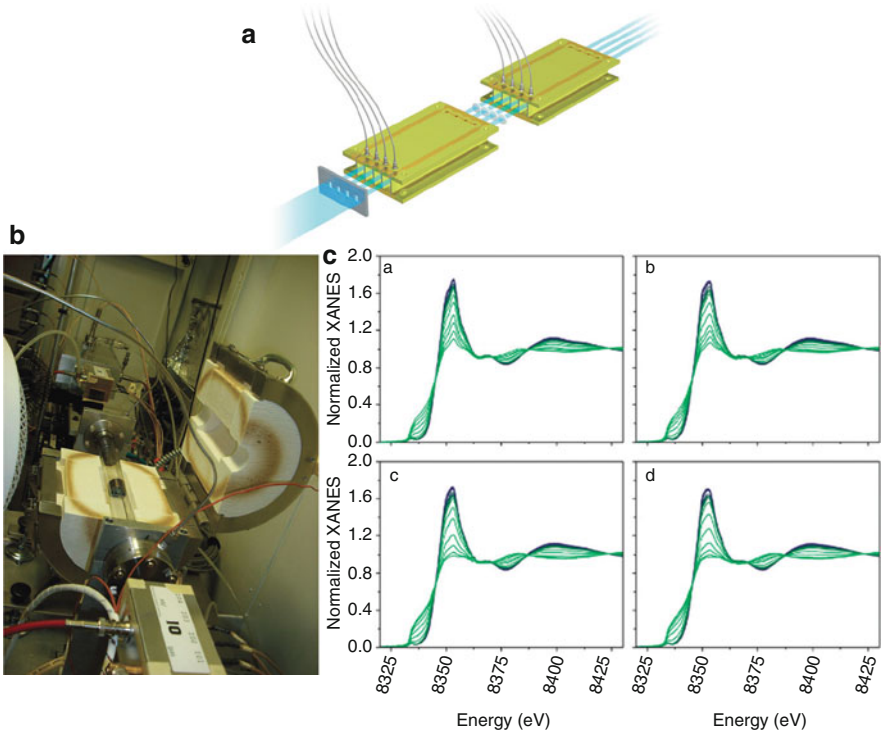

Fig. 5.11 (**a**) Schematic diagram of the experimental setup showing the X-ray beam from the left going through the beam defining aperture, the four samples that are in the path of the four X-ray beams, and the four ionization chambers collecting data. (**b**) Actual experimental setup in the beamline using the quartz tube reactor with the sample holder inside it. The prototype four-channel ion chamber is labeled I0 and is at the front. (**c**) Normalized Ni K-edge temperature-programmed-reduction XANES data collected simultaneously on four Ni-containing catalysts [84]

not change its oxidation state during the reaction. Fe is not present in its metallic form after reduction and during the reaction, but changes in the oxidation state from Fe(II) to Fe(III) occurred during the reaction. QXAS studies were performed to study the real-time transformation of silver species over alumina [90] with a spectrum being collected every second for 30 s. The data taken at Ag K-edge demonstrated the sensitivity of silver to gaseous ethanol. While the reduction of silver occurs at room temperature under air/ethanol flow, it gets accelerated when it is heated to a temperature of 78 °C, the boiling point of ethanol, making Ag-Al_2O_3 catalysts useful for selective catalytic reduction of NO_x in the presence of ethanol. A combination of TPR (temperature programmed reduction) QEXAFS and QXANES along with high resolution TEM, XRD, and diffuse reflectance Fourier transform infrared spectroscopy was used to study water gas shift. It involved detailed characterization and testing of nanoscale ZrO_2 and YSZ supported Pt catalysts [91]. EXAFS results demonstrated that Pt clusters were highly dispersed and similar in size and that Y

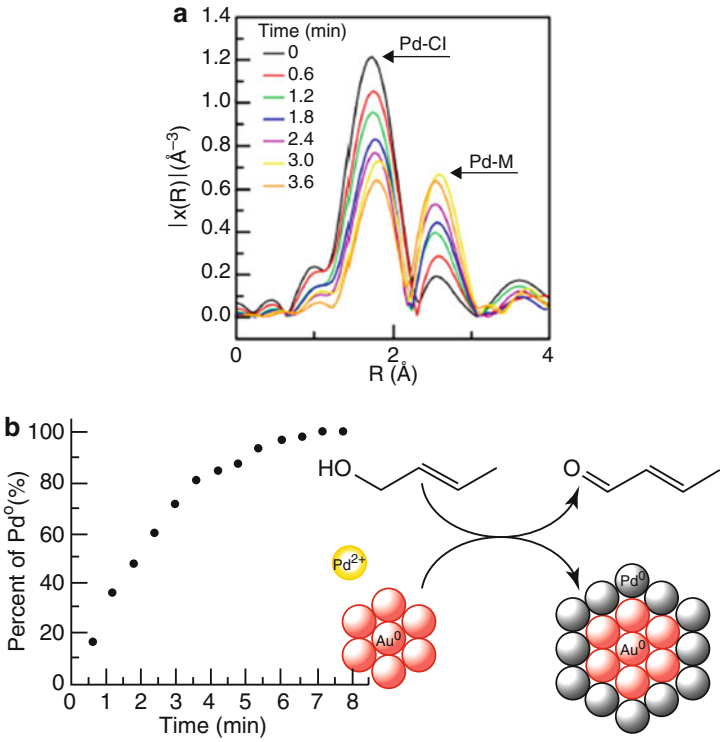

Fig. 5.12 (**a**) Time-resolved Pd K-edge EXAFS data in R-space for the NPs that formed in situ during oxidation of crotyl alcohol in water. (**b**) Growth of Pd shell around Au core with increase in time forming Au core-Pd shell bimetallic catalysts in presence of crotyl alcohol [92]

addition enhanced surface reduction especially in samples with more Zr. Y doped Pt catalysts displayed higher water gas-gas-shift activity relative to the 0.5%Pt/ZrO_2 catalyst when the Y content was below 50%.

In situ Pd K-edge and Pd-L3 edge XAS was used successfully to study the formation of gold core – Pd shell bimetallic NPs from Pd(II) salts in situ in the beam in the presence of crotyl alcohol [92]. Figure 5.12a, b gives time-resolved Pd speciation information which was used to predict the reaction mechanism and kinetics of Pd reducing on the Au NPs and forming Au Core- Pd shell bimetallic nanoparticle catalysts in the presence of crotyl alcohol. These studies also explained the role of Au atoms, which prevented the re-oxidation of the catalytically active Pd atoms present on the surface of the Pd shell around Au core. Thus, we observe that in situ QXAS studies have enriched the field of catalysis immensely. Different types of new cells have been designed in different beamlines around the world, which has in the course of time helped researchers from academics and industry investigate different types of oxidation and reduction mechanisms and the kinetics of the growth of catalysts, thereby accelerating the evolution of novel catalytic materials with tailor made properties.

5.4 In Situ XAS Studies in Nanomaterials with In Situ SAXS and Other Techniques

Construction of next generation synchrotron sources producing beams with enhanced photon flux and the development of faster detectors has led to the growth of many synchrotron-based measurement techniques. Novel experiments have been designed and executed producing unique results in different fields. We have seen so far how in situ XAS characterization techniques have contributed to the fields of catalysis, battery, and in situ chemistry-on-the-beamline for nanomaterials. There have been large-scale developments in the fields of in situ scattering (SAXS) [93, 94], in situ imaging [95], in situ high resolution XRD (HRXRD) [96], and in situ pair distribution function (PDF) measurements also [97, 98]. This initially led to the coupling of ex situ XAS measurements with some of these techniques [99–104]. In the last decade, the efforts to couple in situ XAS measurements with other in situ synchrotron-based techniques have been successful, and this has opened the doors to novel discoveries in various fields, which we shall highlight in this section.

Sasaki et al. have used in situ XRD and in situ XAS to study the synthesis and catalytic activities of carbon supported Ir-Ni core-shell NPs [105]. The NPs, synthesized using chemical reduction followed by thermal annealing, are composed of IrNi alloy cores covered by 2 shells of Ir that protect the Ni core from getting oxidized or modified by the acid electrolyte under elevated potentials. The Ni cores have been found to lead to contraction of the Ir shell, thereby suppressing formation of IrOH on the surface and resulting in a NP system possessing higher H_2 reduction capacity than commercial Pt/C catalysts. The combination of in situ XRD and in situ XAS studies have proved that IrNi core-shell NPs can be a potential candidate for hydrogen anode fuel cell electro-catalysts.

A combination of in situ PDF (pair distribution function) along with XAS was applied to study the structure and nature of PdO-Pd transformation in a 4 wt% Pd/Al_2O_3 catalyst by Keating et al. [106]. Pd phases within the catalyst could be established at various temperatures till 850 °C, above which most of the PdO converted to metallic Pd. Complete re-oxidation of Pd to PdO occurred between 650 °C and 580 °C.

Structural evolution during solid-state formation of Li_2MnO_3, a primary material for Li ion batteries, was investigated by in situ high-energy X-ray diffraction and in situ X-ray absorption spectroscopy [107]. In situ XAS helped to capture formation of an intermediate MnO_2 phase, whereas anisotropic crystallization of Li_2MnO_3 during sintering above 600 °C was observed for in situ diffraction. Without these state-of-the-art techniques, it would not have been possible to study materials for future devices.

In situ XRD and in situ XAS were also used to study the synthesis and oxidation of Co cores of Co-SiO_2 core-shell NPs prepared by sol-gel method [108]. The oxidation was carried out till 800 °C in the presence of air as well as nitrogen. Metallic cobalt as well as a small amount Co in the 2+ state was observed till 200 °C. With an increase in temperature to 300 °C, oxygen from air diffused through SiO_2 and the interface between Co and SiO_2 oxidized to CoO. With further increase in

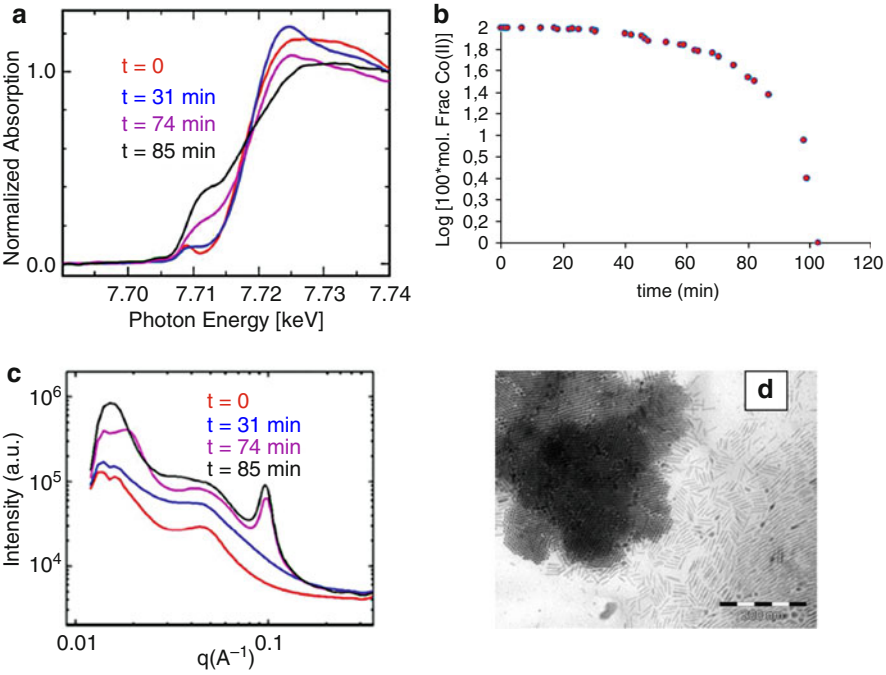

Fig. 5.13 (**a**) Time-dependent Co K-edge QXANES spectra taken at different time intervals during in situ formation of Co nanorods in the beam at 130 °C and 50 psi of H_2, starting with precursor (red) and ending with Co metallic nanorods (black). (**b**) Reduction of Co (II) to Co(0) in the beam. (**c**) In situ SAXS spectra taken during reduction of Co precursor to Co-metallic nanorods in the beam at 130 °C and 50 psi of H_2 and at an energy of 8979 eV. Time intervals for these spectra are same as that for the QXANES spectra. (**d**) TEM image of a superlattice obtained after 3 h of reaction at 130 °C

temperature to 800 °C, Co_3O_4 or a mixture of CoO and Co_3O_4 was formed. Similar phenomenon was observed in the presence of N_2 gas also where the oxygen was procured by Co atoms from the SiO_2 shell. This experiment helped to study the behavior of core-shell NPs at high temperature.

A very unique experiment was done by Cormary et al. [109] to study the detailed growth mechanism and kinetics of cobalt nanorods using in situ SAXS (small angle X-ray scattering) and in situ QXAS measurements. Figure 5.13a, c shows the in situ QXANES and SAXS data taken when the Co (II) precursor reduced to metallic Co nanorods in the presence of a long chain amine and a long chain carboxylic acid. The reaction took place at 130 °C and 50 psi of H_2. Figure 5.13b shows the reduction of Co (+2) to Co(0) with progress in time. Figure 5.13d shows the TEM image of the nanorods produced by the reaction. The growth mechanism starts with a fast nucleation followed by a fast growth brought about by monomer addition. The latter happens during reduction of Co(2+) precursor to Co(0). The last step consists of a slower ripening that occurs after the reduction is complete and the nanorods organized into 3D smectic-like superlattices. An in-depth understanding of the dynamic

processes associated with the nanorod formation could be obtained by these experiments. This will open the gate to synthesize different types of nanomaterial superlattices with tailor made properties.

6 Conclusions and Future Perspective

We have observed that in situ XAS solo and in conjunction with other techniques has developed into a unique tool and has been applied to study local structural changes and mechanisms associated with different types of reactions involving NPs for various applications. In the last couple of years, lots of advancements have occurred in the field of XFEL (X-ray free electron laser) to do XAS measurements in the scale of nano- and picoseconds to study ultrafast reactions happening in nature [110, 111]. Such studies will be extremely beneficial to scientists and engineers to develop novel materials for future generation devices. It has been found that biological samples often get degraded with hard x-rays from an undulator beamline where QXAS is generally done. Efforts should be made so that biological samples can be studied with in situ QXAS to observe reactions occurring in biological organs, organisms and cells [112]. Progress in detector science and enhancement in the design of sample cells will enable in situ QXAS studies along with other in situ techniques to contribute further in the development of nanoscience and nanotechnology.

References

1. Koningsberger DC, Prins R (1988) X-ray absorption, principles, applications, techniques of EXAFS, SEXAFS, XANES. Wiley, New York
2. Müller O, Nachtegaal M, Just J, Lützenkirchen-Hecht D, Frahm R (2016) Quick-EXAFS setup at the SuperXAS beamline for in situ X-ray absorption spectroscopy with 10 ms time resolution. J Synchrotron Radiat 23(1):260–266
3. Prestipino C, Mathon O, Hino R, Beteva A, Pascarelli S (2011) Quick-EXAFS implementation on the general purpose EXAFS beamline at ESRF. J Synchrotron Radiat 18(2):176–182
4. Mathon O, Beteva A, Borrel J, Bugnazet D, Gatla S, Hino R, Kantor I, Mairs T, Munoz M, Pasternak S, Perrin F, Pascarelli S (2015) The time-resolved and extreme condition XAS (TEXAS) facility at the European Synchrotron Radiation Facility: the general-purpose EXAFS bending-magnet beamline BM23. J Synchrotron Radiat 22(6):1548–1554
5. Koide A, Fujikawa T, Ichikuni N (2014) Recent progress in EXAFS/NEXAFS spectroscopy. J Electron Spectrosc Relat Phenom 195:375–381
6. Dent AJ (2002) Development of time-resolved XAFS instrumentation for quick EXAFS and energy-dispersive EXAFS measurements of catalyst systems. Top Catal 18(1–2):14–22
7. Segre CU, Leyarovska NE, Chapman LD, Lavender WM, Plag PW, King AS, Kropf AJ, Bunker BA, Kemner KM, Dutta P, Duran RS, Kaduk J (2000) The MRCAT insertion device beamline at the advanced photon source. AIP Conf Proc 521(1):419–422
8. Newville M (2004) Fundamentals of XAFS. Consortium for advanced radiation sources, University of Chicago, Chicago. http://XAFS.org/
9. Lee PA, Citrin PH, Eisenberger P, Kincaid BM (1981) Extended X-ray absorption fine structure – its strengths and limitations as a structural tool. Rev Mod Phys 53(4):769
10. Rehr JJ, Albers RC (2000) Theoretical approaches to X-ray absorption fine structure. Rev Mod Phys 72(3):621

11. Bunker G (2010) Introduction to XAFS: a practical guide to X-ray absorption fine structure spectroscopy, 1st edn. Cambridge University Press, Cambridge
12. Kelly SD, Hesterberg D, Ravel B (2008) Chapter 14 Analysis of soils and minerals using X-ray absorption spectroscopy. In: Methods of soil analysis Part 5 – Mineralogical methods. Soil Science Society of America, Madison, pp 387–463
13. Ravel B, Newville M (2005) ATHENA, ARTEMIS, HEPHAESTUS: data analysis for X-ray absorption spectroscopy using IFEFFIT. J Synchrotron Radiat 12(4):537–541
14. Zabinsky SI, Rehr JJ, Andukinov A, Albers RC, Ellen MJ (1995) Multiple-scattering calculations of X-ray absorption spectra. Phys Rev B 52(4):2995
15. Kumar CSSR (ed) (2010) Microfluidic devices in nanotechnology – fundamental concepts. Wiley, Hoboken
16. Kumar CSSR (ed) (2010) Microfluidic devices in nanotechnology – applications. Wiley, Hoboken
17. Gaur S, Miller JT, Stellwagen DR, Sanampudi A, Kumar CSSR, Spivey JJ (2012) Synthesis, characterization and testing of supported Au catalysts prepared from atomically-tailored $Au_{38}(SC_{12}H_{25})_{24}$ clusters. Phys Chem Chem Phys 14(5):1627–1634
18. Biswas S, Miller JT, Li Y, Nandakumar K, Kumar CSSR (2012) Developing a millifluidic platform for the synthesis of ultra-small nano-clusters: ultra-small copper nano-clusters as a case study. Small 8(5):688–698
19. Krishna KS, Navin CV, Biswas S, Singh V, Ham K, Bovenkamp GL, Theegala CS, Miller JT, Spivey J, Kumar CSSR (2013) Milli-fluidics for time-resolved mapping of the growth of gold nanostructures. J Am Chem Soc 135(14):5450–5456
20. Krishna KS, Biswas S, Navin CV, Yamane DG, Miller JT, Kumar CSSR (2013) Millifluidics for chemical synthesis and time-resolved mechanistic studies. J Vis Exp 81:e50711
21. Navin CV, Krishna KS, Bovenkamp GL, Miller JT, Chattopadhyay S, Shibata T, Losovyj Y, Singh V, Theegala C, Kumar CSSR (2015) Investigation of the synthesis and characterization of platinum-DMSA nanoparticles using millifluidic chip reactor. Chem Eng J 281:81–86
22. Yin Y, Alivisatos AP (2005) Colloidal nanocrystal synthesis and the organic–inorganic interface. Nature 437(7059):664–670
23. Pellegrino T, Kudera S, Liedl T, Javier AM, Manna L, Parak WJ (2005) On the development of colloidal nanoparticles towards multifunctional structures and their possible use for biological applications. Small 1(1):48–63
24. Talapin DV, Lee J-S, Kovalenko MV, Shevchenko EV (2010) Prospects of colloidal nanocrystals for electronic and optoelectronic applications. Chem Rev 110(1):389–458
25. Park J, Joo J, Kwon SG, Jang Y, Hyeon T (2007) Synthesis of monodisperse spherical nanocrystals. Angew Chem Int Ed 46(25):4630–4660
26. Kwon SG, Krylova G, Phillips PJ, Klie RF, Chattopadhyay S, Shibata T, Bunel EE, Liu Y, Prakapenka VB, Lee B, Shevchenko EV (2015) Heterogeneous nucleation and shape transformation of multicomponent metallic nanostructures. Nat Mater 14(2):215–223
27. Kwon SG, Chattopadhyay S, Koo B, dos Santos Claro PC, Shibata T, Requejo FG, Giovanetti LJ, Johnson C, Prakapenka V, Lee B, Shevchenko EV (2016) Oxidation induced doping of nanoparticles revealed by in situ X-ray adsorption studies. Nano Lett 16(6):3738–3747
28. McPeak KM, Becker MA, Britton NG, Majidi H, Bunker BA, Baxter JB (2010) In situ X-ray absorption near-edge structure spectroscopy of ZnO nanowire growth during chemical bath deposition. Chem Mater 22(22):6162–6170
29. Song J, Zhang J, Xie Z, Wei S, Pan Z, Hu T, Xie Y (2010) In situ XAFS studies on the growth of ZnSe quantum dots. Nucl Instrum Methods Phys Res, Sect A 619(1–3):280–282
30. Yan H, Mayanovic RA, Demster JW, Anderson AJ (2013) In situ monitoring of the adsorption of Co^{2+} on the surface of Fe_3O_4 nanoparticles in high-temperature aqueous fluids. J Supercrit Fluids 81:175–182
31. Tryk DA, Bae IT, Hu Y, Kim S, Antonio MR, Schersona DA (1995) In situ X-ray absorption fine structure measurements of $LaNi_5$ electrodes in alkaline electrolytes. J Electrochem Soc 142(3):824–828

32. Shiraishi Y, Nakai I, Tsubata T, Himeda T, Nishikawa F (1997) In situ transmission X-ray absorption fine structure analysis of the charge–discharge process in $LiMn_2O_4$, a rechargeable lithium battery material. J Solid State Chem 133(2):587–590
33. Balasubramanian M, Sun X, Yang XQ, McBreen J (2001) In situ X-ray diffraction and X-ray absorption studies of high-rate lithium-ion batteries. J Power Sources 92(1–2):1–8
34. Terada Y, Yasaka K, Nishikawa F, Konishi T, Yoshio M, Nakai I (2001) In situ XAFS analysis of $Li(Mn,M)_2O_4$ (M = Cr, Co, Ni) 5V cathode materials for lithium-ion secondary batteries. J Solid State Chem 156(2):286–291
35. Kropf AJ, Tostmann H, Johnson CS, Vaughey JT, Thackeray MM (2001) An in situ X-ray absorption spectroscopy study of InSb electrodes in lithium batteries. Electrochem Commun 3 (5):244–251
36. Balasubramanian M, McBreen J, Davidson IJ, Whitfield PS, Kargina I (2002) In situ X-ray absorption study of a layered manganese-chromium oxide-based cathode material. J Electrochem Soc 149(2):A176–A184
37. Johnson CS, Kropf AJ (2002) In situ XAFS analysis of the $Li_xNi_{0.8}Co_{0.2}O_2$ cathode during cycling in lithium batteries. Electrochim Acta 47(19):3187
38. Holzapfel M, Proux O, Strobel P, Darie C, Borowski M, Morcrette M (2004) Effect of iron on delithiation in $Li_xCo_{1-y}Fe_yO_2$: part 2, in-situ XANES and EXAFS upon electrochemical cycling. J Mater Chem 14(1):102–110
39. Yoon W-S, Balasubramanian M, Chung KY, Yang X-Q, McBreen J, Grey CP, Fischer DA (2005) Investigation of the charge compensation mechanism on the electrochemically Li-ion deintercalated $Li_{1-x}Co_{1/3}Ni_{1/3}Mn_{1/3}O_2$ electrode system by combination of soft and hard X-ray absorption spectroscopy. J Am Chem Soc 127(49):17479–17487
40. Deb A, Bergmann U, Cramer SP, Cairns EJ (2005) In-situ X-ray absorption spectroscopic study of the Li $[Ni_{1/3}Co_{1/3}Mn_{1/3}]O_2$ cathode material. J Appl Phys 97(11):113523
41. Deb A, Cairns EJ (2006) In situ X-ray absorption spectroscopy – a probe of cathode materials for Li-ion cells. Fluid Phase Equilib 241(1–2):4–19
42. Dominko R, Arčon I, Kodre A, Hanžel D, Gaberšček M (2009) In-situ XAS study on Li_2MnSiO_4 and Li_2FeSiO_4 cathode materials. J Power Sources 189(1):51–58
43. Nedoseykina T, Kim MG, Park S-A, Kim H-S, Kim S-B, Cho J, Lee Y (2010) In situ X-ray absorption spectroscopic study for the electrochemical delithiation of a cathode $LiFe_{0.4}Mn_{0.6}PO_4$ material. Electrochim Acta 55(28):8876–8882
44. Ito A, Sato Y, Sanada T, Hatano M, Horie H, Ohsawa Y (2011) In situ X-ray absorption spectroscopic study of Li-rich layered cathode material $Li[Ni_{0.17}Li_{0.2}Co_{0.07}Mn_{0.56}]O_2$. J Power Sources 196(16):6828–6834
45. Simonin L, Colin J-F, Ranieri V, Canévet E, Martin J-F, Bourbon C, Baehtz C, Strobel P, Daniel L, Patoux S (2012) In-situ investigations of a Li-rich Mn-Ni layered oxide for Li-ion batteries. J Mater Chem 22(22):11316–11322
46. Love CT, Korovina A, Patridge CJ, Swider-Lyons KE, Twigg ME, Ramaker DE (2013) Review of $LiFePO_4$ phase transition mechanisms and new observations from X-ray absorption spectroscopy. J Electrochem Soc 160(5):A3153–A3161
47. Pohl AH, Guda AA, Shapovalov VV, Witte R, Das B, Scheiba F, Rothe J, Soldatov AV, Fichtner M (2014) Oxidation state and local structure of a high-capacity $LiF/Fe(V_2O_5)$ conversion cathode for Li-ion batteries. Acta Mater 68:179–188
48. Hirsch O, Zeng G, Luo L, Staniuk M, Abdala PM, van Beek W, Rechberger F, Süess MJ, Niederberger M, Koziej D (2014) Aliovalent Ni in MoO lattice – probing the structure and valence of Ni and its implication on the electrochemical performance. Chem Mater 26 (15):4505–4513
49. Pelliccione CJ, Ding Y, Timofeeva EV, Segre CU (2015) In situ XAFS study of the capacity fading mechanisms in ZnO anodes for lithium-ion batteries. J Electrochem Soc 162(10): A1935–A1939

50. Li B, Shao R, Yan H, An L, Zhang B, Wei H, Ma J, Xia D, Han X (2016) Understanding the stability for Li-rich layered oxide Li_2RuO_3 cathode. Adv Funct Mater 26(9):1330–1337
51. Mansour AN, Badway F, Yoon WS, Chung KY, Amatucci GG (2010) In situ X-ray absorption spectroscopic investigation of the electrochemical conversion reactions of CuF_2-MoO_3 nanocomposite. J Solid State Chem 183(12):3029–3038
52. Pelliccione CJ, Timofeeva EV, Segre CU (2016) Potential-resolved in situ X-ray absorption spectroscopy study of Sn and SnO nanomaterial anodes for lithium-ion batteries. J Phys Chem C 120(10):5331–5339
53. Pellicione CJ, Timofeeva EV, Segre CU (2015) In situ X-ray absorption spectroscopy study of the capacity fading mechanism in hybrid $Sn_3O_2(OH)_2$/graphite battery anode nanomaterials. Chem Mater 27(2):574–580
54. Patridge CJ, Love CT, Swider-Lyons KE, Twigg ME, Ramaker DE (2013) In-situ X-ray absorption spectroscopy analysis of capacity fade in nanoscale-$LiCoO_2$. J Solid State Chem 203:134–144
55. Pelliccione CJ, Li YR, Marschilok AC, Takeuchi KJ, Takeuchi ES (2016) X-ray absorption spectroscopy of lithium insertion and de-insertion in copper birnessite nanoparticle electrodes. Phys Chem Chem Phys 18(4):2959–2967
56. Koo B, Xiong H, Slater MD, Prakapenka VB, Balasubramanian M, Podsiadlo P, Johnson CS, Rajh T, Shevchenko EV (2012) Hollow iron oxide nanoparticles for application in lithium ion batteries. Nano Lett 12(5):2429–2435
57. Koo B, Goli P, Sumant AV, dos Santos Claro PC, Rajh T, Johnson CS, Balandin AA, Shevchenko EV (2014) Toward lithium ion batteries with enhanced thermal conductivity. ACS Nano 8(7):7202–7207
58. Koo B, Chattopadhyay S, Shibata T, Prakapenka VB, Johnson CS, Rajh T, Shevchenko EV (2013) Intercalation of sodium ions into hollow iron oxide nanoparticles. Chem Mater 25 (2):245–252
59. Iwasawa Y (1997) Applications of X-ray absorption fine structure to catalysts and model surfaces. J Phys IV 7(C2):67–81
60. Mukerjee S, McGreen J (1999) An in-situ X-ray absorption spectroscopy investigation of the effect of Sn additions to carbon-supported Pt electrocatalysts, part 1. J Electrochem Soc 146 (2):600–606
61. Bazin D, Mottet C, Tréglia G, Lynch J (2000) New trends in heterogeneous catalysis processes on metallic clusters from synchrotron radiation and theoretical studies. Appl Surf Sci 164 (1–4):140–146
62. Bazin D, Mottet C, Tréglia G (2000) New opportunities to understand heterogeneous catalysis processes on nanoscale bimetallic particles through synchrotron radiation and theoretical studies. Appl Catal A Gen 200:47–54
63. Lee JS, Park ED (2002) In-situ XAFS characterization of supported homogeneous catalysts. Top Catal 18(1–2):67–72
64. Bazin D (2002) Solid state concepts to understand catalysis using nanoscale metallic particles. Top Catal 18(1–2):79–84
65. Grunwaldt JD, Wandeler R, Baiker A (2003) Supercritical fluids in catalysis: opportunities of in-situ spectroscopic studies and monitoring phase behavior. Catal Rev Sci Eng 45(1):1–96
66. Bazin D, Rehr J (2003) Soft X-ray absorption spectroscopy at the cutting edge for nanomaterials used in heterogeneous catalysis: the state of the art. Catal Lett 87(1–2):85–90
67. Bare SR, Ressler T (2009) Chapter 6 characterization of catalysts in reactive atmospheres by X-ray absorption spectroscopy. Adv Catal 52:339–465
68. Grunwaldt JD (2009) Shining X-rays on catalysts at work. J Phys Conf Ser 190(1):012151
69. Andrew J, Lobo RF (2010) Identifying reaction intermediates and catalytic active sites through in situ characterization techniques. Chem Soc Rev 39(12):4783–4793

70. Singh J, Lamberti C, van Bokhoven JA (2010) Advanced X-ray absorption and emission spectroscopy: in situ catalytic studies. Chem Soc Rev 39(12):4754–4766
71. Pascarelli S, Mathon O (2010) Advances in high brilliance energy dispersive X-ray absorption spectroscopy. Phys Chem Chem Phys 12(21):5535–5546
72. Ferri D, Newton MA, Nachtegaal M (2011) Modulation excitation X-ray absorption spectroscopy to probe surface species on heterogeneous catalysts. Top Catal 54(16–18):1070–1078
73. Fechetea I, Wangb Y, Vedrinec JC (2012) The past, present and future of heterogeneous catalysis. Catal Today 189(1):2–27
74. Frenkel AI (2012) Applications of extended X-ray absorption fine-structure spectroscopy to studies of bimetallic nanoparticle catalysts. Chem Soc Rev 41(24):8163–8178
75. Wachs IE (2013) Catalysis science of supported vanadium oxide catalysts. Dalton Trans 42(33):11762–11769
76. Ehteshami SMM, Chan SH (2013) A review of electrocatalysts with enhanced CO tolerance and stability for polymer electrolyte membrane fuel cells. Electrochim Acta 93:334–345
77. Grunwaldt J-D, Wagner JB, Dunin-Barkowski RE (2013) Imaging catalysts at work: a hierarchical approach from the macro-to the meso- and nano-scale. ChemCatChem 5(1):62–80
78. Nemeth L, Bare SR (2014) Science and technology of framework metal containing zeotype catalysts. Adv Catal 57:1–97
79. Garino C, Borfecchia E, Gobetto R, van Bokhoven JA, Lamberti C (2014) Determination of the electronic and structural configuration of coordination compounds by synchrotron-radiation techniques. Coord Chem Rev 277:130–186
80. Tielens F, Bazin D (2015) Operando characterization and DFT modelling of nanospinels: some examples showing the relationship with catalytic activity. Appl Catal A Gen 504:631–641
81. Sherborne GJ, Nguyen BN (2015) Recent XAS studies into homogeneous metal catalyst in fine chemical and pharmaceutical syntheses. Chem Cent J 9(1):37
82. Zhu M, Wachs IE (2015) Iron-based catalysts for the high-temperature water gas shift (HT-WGS) reaction: a review. ACS Catal 6(2):722–732
83. Meneses CT, Flores WH, Sotero AP, Tamura E, Garcia F, Sasaki JM (2006) In situ system for X-ray absorption spectroscopy experiments to investigate nanoparticle crystallization. J Synchrotron Radiat 13(6):468–470
84. Bare SR, Kelly SD, Ravel B, Greenlay N, King L, Mickelson GE (2010) Characterizing industrial catalysts using in situ XAFS under identical conditions. Phys Chem Chem Phys 12(27):7702–7711
85. Nelson RC, Miller JT (2012) An introduction to X-ray absorption spectroscopy and its in situ application to organometallic compounds and homogeneous catalysts. Catal Sci Technol 2(3):461–470
86. Rochet A, Moizan V, Pichon C, Diehl F, Berliet A, Briois V (2011) In situ and operando structural characterization of a Fischer-Tropsch supported cobalt catalyst. Catal Today 171(1):186–191
87. O'Neill BJ, Miller JT, Dietrich PJ, Sollberger FG, Ribeiro FH, Dumesic JA (2014) Operando X-ray absorption spectroscopy studies of sintering for supported copper catalysts during liquid-phase reaction. ChemCatChem 6(9):2493–2496
88. Grunwaldt J-D, Caravati M, Hannemann S, Baiker A (2004) X-ray absorption spectroscopy under reaction conditions: suitability of different reaction cells for combined catalyst characterization and time-resolved studies. Phys Chem Chem Phys 6:3037–3047
89. Kumar A, Miller JT, Mukasyan AS, Wolf EE (2013) In situ XAS and FTIR studies of a multicomponent Ni/Fe/Cu catalyst for hydrogen production from ethanol. Appl Catal A Gen 467:593–603
90. Sayah E, Fontaine CL, Briois V, Brouri D, Massiani P (2012) Silver species reduction upon exposure of Ag/Al_2O_3 catalyst to gaseous ethanol: an in situ quick-XANES study. Catal Today 189(1):155–159

91. Martinelli M, Jocabs G, Graham UM, Shafer WD, Cronauer DC, Kropf AJ, Marshall CL, Khalid S, Visconti CG, Letti L, Davis BH (2015) Water-gas shift: characterization and testing of nanoscale YSZ supported Pt catalysts. Appl Catal A Gen 497:184–197
92. Maclennan A, Banerjee A, Hu Y, Miller JT, Scott RWJ (2013) In situ X-ray absorption spectroscopic analysis of gold–palladium bimetallic nanoparticle catalysts. ACS Catal 3(6):1411–1419
93. Craievich AF (2002) Synchrotron SAXS studies of nanostructured materials and colloidal solutions. A review. Mater Res 5(1):1–11
94. Abécassis B, Testard F, Spalla O, Barboux P (2007) Probing in situ the nucleation and growth of gold nanoparticles by small-angle X-ray scattering. Nano Lett 7(6):1723–1727
95. Susini J, Salome M, Fayward B, Ortega R, Kaulich B (2002) The scanning X-ray microprobe at the ESRF X-ray microscopy beamline. Surf Rev Lett 9(1):203–211
96. Wu J, Shan S, Petkov V, Prasai B, Cronk H, Joseph P, Luo J, Zhong C-J (2015) Composition-structure-activity relationships for palladium-alloyed nanocatalysts in oxygen reduction reaction: an ex-situ/in-situ high energy X-ray diffraction study. ACS Catal 5(9):5317–5327
97. Beyer KA, Zhao H, Borkiewicz OJ, Newton MA, Chupas PJ, Chapman KW (2014) Simultaneous diffuse reflection infrared spectroscopy and X-ray pair distribution function measurements. J Appl Crystallogr 47(1):95–101
98. Chapman KW (2016) Emerging operando and X-ray pair distribution function methods for energy materials developments. MRS Bull 41(3):231–240
99. Oxford SM, Lee PL, Chupas PJ, Chapman KW, Kung MC, Kung HH (2010) Study of supported PtCu and PdAu bimetallic nanoparticles using in-situ X-ray tools. J Phys Chem 114(40):17085–17091
100. Newton MA, van Beek W (2010) Combining synchrotron-based X-ray techniques with vibrational spectroscopies for the in situ study of heterogeneous catalysts: a view from a bridge. Chem Soc Rev 39(12):4845–4863
101. Ehrlich SN, Henson JC, Camara AL, Bariio L, Estralla M, Zhou G, Si R, Khalid S, Wang Q (2011) Combined XRD and XAS. Nucl Inst Methods Phys Res A 649(1):213–215
102. Gallagher JR, Li T, Zhao H, Liu J, Lei Y, Zhang X, Ren Y, Elam JW, Meyer RJ, Winans RE, Miller JT (2014) In situ diffraction of highly dispersed supported platinum nanoparticle. Catal Sci Technol 4(9):3053–3063
103. Gallagher JR, Childers DJ, Zhao H, Winans RE, Meyer RJ, Miller JT (2015) Structural evolution of an intermetallic Pd-Zn catalyst selective for propane dehydrogenation. Phys Chem Chem Phys 17(42):28144–28153
104. Muñoz FF, Cabezas MD, Acuña LM, Leyva AG, Baker RT, Fuentes RO (2011) Structural properties and reduction behavior of novel nanostructured Pd/gadolinia-doped ceria catalysts with tubular morphology. J Phys Chem C 115(17):8744–8752
105. Sasaki K, Kuttiyiel KA, Barrio L, Su D, Frenkel AI, Marinkovic N, Mahajan D, Adzic RR (2011) Carbon-supported IrNi core-shell nanoparticles: synthesis, characterization, and catalytic activity. J Phys Chem C 115(20):9894–9902
106. Keating J, Sankar G, Hyde TI, Kohara S, Ohara K (2013) Elucidation of structure and nature of the PdO–Pd transformation using in situ PDF and XAS techniques. Phys Chem Chem Phys 15(22):8555–8565
107. Kan Y, Hu Y, Croy J, Ren Y, Sun C-J, Heald SM, Bareño J, Bloom I, Chen Z (2014) Formation of Li_2MnO_3 investigated by in situ synchrotron probes. J Power Sources 266:341–346
108. Zhang K, Zhao Z, Wu Z, Zhou Y (2015) Synthesis and detection the oxidization of Co cores of Co@SiO_2 core-shell nanoparticles by in situ XRD and EXAFS. Nanoscale Res Lett 10(1):37
109. Cormary B, Li T, Liakakos N, Peres L, Fazzini P-F, Blon T, Respaud M, Kropf AJ, Chaudret B, Miller JT, Mader EA, Soulantica K (2016) Concerted growth and ordering of

cobalt nanorod arrays as revealed by tandem in situ SAXS-XAS studies. J Am Chem Soc 138(27):8422–8431
110. Penfold TJ, Milne CJ, Chergui M (2013) Recent advances in ultrafast X-ray spectroscopy of solutions. In: Rice SA, Dinner AR (eds) Advances in chemical physics, 2nd edn. Wiley, Hoboken, pp 1–41
111. Borfecchia E, Garino C, Salassa L, Lamberti C (2013) Synchrotron ultrafast techniques for photoactive transition metal complexes. Phil Trans R Soc A 371:20120132. https://doi.org/10.1098/rsta.2012.0132
112. Ortega R (2012) X-ray absorption spectroscopy of biological samples. A tutorial. J Anal At Spectrom 27(12):2054–2065